

An Augmented Reality System for Liver Thermal Ablation: Design and Evaluation on Clinical Cases

S.A. Nicolau^a X. Pennec^b L. Soler^a X. Buy^c A. Gangi^c
N. Ayache^b J. Marescaux^a

^a*IRCAD, 1 place de l'hopital, 67091, Strasbourg France*

^b*INRIA 2004 route des Lucioles - BP 93 06902 Sophia Antipolis Cedex France*

^c*Department of Radiology, University Louis Pasteur, Strasbourg, France*

Abstract

We present in this paper an augmented reality guidance system for liver thermal ablation in interventional radiology. To show the relevance of our methodology, the system is incrementally evaluated on an abdominal phantom and then on patients in the operating room. The system registers in a common coordinate system a preoperative image of the patient and the position of the needle that the practitioner manipulates. The breathing motion uncertainty is taken into account with a respiratory gating technique: the preoperative image and the guidance step are synchronized on expiratory phases. In order to fulfil the real-time constraints, we have developed and validated algorithms that automatically process and extract feature points. Since the guidance interface is also a major component of the system effectiveness, we validate the overall targeting accuracy on an abdominal phantom. This experiment showed that a practitioner can reach a predefined target with an accuracy of 2 mm with an insertion time below one minute. Finally, we propose a passive evaluation protocol of the overall system in the operating room during five interventions on patients. These experiments show that the system can provide a guidance information during expiratory phases with an error below 5 mm.

Key words: augmented reality, computer-guided system, liver punctures, 3D/2D registration, breathing motion

PACS:

1 Introduction

1.1 Medical context and purposes

The treatment of liver tumors by minimally invasive techniques, such as Radio-Frequency (RF) thermal ablation, begins to be widely used [1,2]. However, the guidance procedure to reach the tumors with the needle is still realized visually with per-operative 2D cross-sections of the patient using either Ultrasound (US), Computed Tomography (CT) or Magnetic Resonance (MR) images displayed on a monitor: positioning correctly the needle using this suboptimal 2D information is always a challenging task for the practitioner. Moreover, each guidance modality has its own drawbacks. CT/MRI guidance needs repetitive acquisitions for needle adjustment and sometimes several reinsertion attempts. This lengthens the intervention duration, and increases post procedure complications and radiation exposure (when CT-guided). In addition, the MRI gantry diameter is small and does not permit the manipulation of long needles (used when the tumor is deep inside the patient). Finally, US guidance needs strong medical experience for image understanding, and tumors lying under the ribs are hardly visible and cannot be targeted.

In this paper, we aim at developing a guidance system for thermal ablation of liver tumors in interventional radiology. To guarantee the liability of such a system, it is of the upper importance to validate the accuracy in real conditions on patients.

1.2 Clinical requirements

A recent report shows that RF thermal ablation has to be performed on tumors with a diameter between 1 and 3 cm [3]. Thus, our radiologists consider that a guidance system has to provide an accuracy better than 5 mm to avoid destroying too much healthy cells when the needle tip is not perfectly centered in the tumor. Moreover, since a conventional insertion lasts between 10 and 40 minutes, the system interface has to allow an insertion duration below 10 minutes. The system also has to be adapted to the operating room requirements (cumbersomeness and sterility). This means that all foreign bodies must be sterile if they have to be close to the patient during the needle insertion. In addition, since the guiding accuracy depends on numerous parameters, the system has to detect any algorithm failure to ensure the gesture guidance. For instance, the practitioner may perform a dangerous movement if the system assumes a static patient and does not detect that the latter slid several millimetres on the table.

1.3 Related works

Numerous works have been carried out to help practitioners during percutaneous punctures. There are two global approaches: robotized and manual.

Concerning the robotized approach, several labs [4–9] propose a needle guidance toward a target in the patient, who lies on the CT-table. The robotic arm being calibrated beforehand in the CT reference frame, the target is defined in the intra-operative image and the robotic arm automatically orientates the needle toward it. Then, the practitioner manually inserts the needle until the system warns that the target is reached. The feasibility of the approach was demonstrated on phantoms. The authors reasonably think that their system should work on man if a respiratory gating technique is used to compensate for breathing motion (that can induce deformations above 3 cm [10]). To our knowledge, only the system in [6] was evaluated in a randomised patient study. Results showed that the robotic arm reduced the insertion duration and the radiation exposure. However, accuracy results were only reported on a phantom and not on patients. As a consequence, the breathing motion influence on the accuracy could not be quantified.

Manual approaches to guide practitioners can be classified according to the image modality: US, X-ray, CT and MRI. Some labs [11–13] propose a US-guided system that displays in real-time the acquired US slice in the operator field of view. In-vivo validation showed the usefulness of the techniques. However, a correct interpretation of the features in US images requires a skilled practitioner and tumors are sometimes not visible with US modality. Finally, the displayed augmented information is only 2-dimensional, increasing the difficulty of understanding the 3D relative position of the structures of interest.

Mitschke et al. [14] and Bascle et. al. [15] propose a needle guidance system using an X-ray C-arm. A camera attached to the C-arm provides a video image of the patient augmented by the X-ray image. The registration quality is ensured by a mirror calibration that superimposes both optical centers of the camera and of the X-ray source. To localize the target, two X-ray images have to be taken at 2 different positions, and a particular device holding the needle is necessary to orientate it correctly. The guiding accuracy of this system was validated on a phantom and on a cadaveric animal limb. Then, this ingenious system automatically provides the right orientation toward the target, but cannot account for any movement of the patient unless two new C-arm acquisitions are done. One of the limitations is that a 2D X-ray does not allow the practitioner to see the critical structures (like vessels) that will be crossed by the needle. For liver percutaneous puncture, this kind of information is necessary to avoid any complication.

Fichtinger et al. recently developed a system for conventional CT-scanner to assist needle placement [16,17]. It displays in the practitioner field of view one axial CT slice acquired intra-operatively, thereby providing a 2D internal view of the patient. Although the system is rather easy to be set up in the operating room, its application to the liver is limited since the practitioner has to reach the target with a path that belongs to the displayed slice. Thus this can result into a suboptimal path. Moreover, since the needle has to remain in the displayed axial slice, some zones in the liver cannot be reached by the needle without crossing a critical structure.

In the context of MRI-guided needle punctures, Vogt et al. displays in a Head-Mounted-Display (HMD) the target (defined in a preoperative MRI image) and the needle position at the same time [18]. They report a targeting accuracy of 1 cm on a living pig (against 3 mm on a static phantom) which is explained by the use of a rigid registration (to relate HMD and MRI frames) despite the breathing motion.

To summarise, part of the systems may be inadequate to liver constraints and very few systems have been evaluated on patients. This is not surprising since such an evaluation is very hard to set up: an Institutional Review Board (IRB) approval is needed so that the medical protocol can be modified. The alternative way is to elaborate a passive evaluation protocol riskless for the patient with a ground truth that is hardly available in standard clinical conditions. Only the robotic system in [6] has been tested on patients to evaluate its benefits in clinical conditions. Unfortunately the accuracy that can be reached in their conditions was not measured. Although a clinical benefit evaluation is mandatory, we do think that it is also crucial to know the minimal system accuracy available in clinical conditions: it allows practitioners to evaluate the risk of their movements during insertion when the needle is close to critical structures.

In previous works [19], we have developed a guidance system for liver thermal ablation based on a preoperative CT image. The system was designed so that it does not constrain radiologists when they choose the needle path toward the target. We showed on a static abdominal phantom that the targeting accuracy was about 2.5 mm. Obviously, the patient is not static, yet we believe like others [7,16,6,18] that pseudo-static conditions can be provided using a respiratory gating technique, i.e. the preoperative CT and the computer guidance are realized at the same point of the breathing cycle (generally expiration). This reasonable assumption is based on clinical studies performed on the organ repositioning error of a patient under breathing monitoring (intubation, ABC control or active apnea) evaluated below 2 mm [20–24]. However, it has to be highlighted that these experiments were performed in controlled conditions (volunteers were not to undergo a heavy intervention), and within a delay that may not fit clinical conditions. For example, needle insertion du-

ration can reach 40 minutes if the target is badly located. To our knowledge, no experiment shows the reproducibility for such a long duration. Moreover, gas in bowels and viscera may move during the intervention, disturbing the pseudo-static assumption. Last but not least, the needle is tracked optically by our system and the needle tip accuracy can be ensured to be below 1 mm provided that it remains perfectly straight during the insertion. Even if the practitioner inserts it and thinks it remains straight, this is questionable. This is why we think that an accuracy evaluation of the whole system on patients in clinical conditions is mandatory.

1.4 Contributions and overview of the paper

In [19], we presented a guidance system in interventional CT for liver thermal ablation that had been evaluated on a phantom only. In this paper, we present a new version of our guidance system, each part being evaluated on real data. Firstly, we have developed and evaluated a new guidance interface on an abdominal phantom. Then, we have designed a passive protocol that allows to evaluate on patients in clinical conditions the needle bending, the organ and skin repositioning error and the whole system error (that includes needle tracking, patient registration and patient repositioning error). Finally, experiments showed that despite needle bending and organ repositioning error, a global accuracy within 5 mm is reachable in clinical conditions.

The paper is divided into three parts. In Sec. 2, we present the system principles and describe the respiratory gating technique we use. In Sec. 3, we perform an evaluation of the new guidance interface on an abdominal phantom to show that the system is accurate and ergonomic. This experiment demonstrates that the in-vitro targeting accuracy is below 2 mm with an insertion duration under 30 sec. In Sec. 4, we detail our riskless passive protocol to clinically evaluate our system and present our results on patients that show the system can provide a guidance information that fits clinical requirements.

2 Principles of our guidance system

In our setup, the patient is under general anesthesia (70% of hepatic thermal ablation at the Strasbourg Hospital)¹. and 15 radio-opaque ring markers are stuck on his abdomen. Then, a CT-scan is acquired just before the

¹ Unfortunately, we did not find any statistic paper on the percentage of hepatic ablation under general anesthesia. However, some review papers on thermal ablation of hepatic carcinoma seem to confirm our local statistic [25,26].

intervention. A 3D-reconstruction of the structures of interest (skin, liver, tumors, radio-opaque markers) is performed [27] (in the latter, we call this 3D-reconstruction the patient model). A black dot is printed into each marker and they are removed from the skin (cf. Fig. 1): this is necessary since they are not sterile. Two jointly calibrated cameras are viewing the patient skin from two different angles of view. They are used for two purposes: firstly to track the needle manipulated by the practitioner, secondly to register the patient model in the camera frame using the black dot markers visible in both video images. This allows us to provide the practitioner with the relative position of the needle with respect to the patient model.



Fig. 1. Left: ring radio-opaque markers are stuck on the patient skin. Right: black dot is printed in each marker. Since patient skin is sterilized with betadine and alcohol, an indelible pen has to be used.

In this section, we firstly explain our respiratory gating technique to compensate for the breathing motion. The used method implies heavy time constraints that led us to provide a fast registration of the patient model. Then, we summarise the algorithms allowing to register the patient and track the needle at a sufficient time rate.

2.1 Taking the patient motion into account

To reach accuracy (5 mm) and safety requirements, the patient motion during the intervention must not be neglected. There are two kinds of movements that have to be tracked and compensated: a global movement of the patient (sliding for example) and the breathing deformation. To detect a global movement we follow the position of the black dot markers with the video camera. This movement tracking is done at 10 Hz (see next subsection for the tracking algorithm). If the system detects any movement that reduces the accuracy, the practitioner is informed. To compensate for the breathing deformation, we propose to use a respiratory gating technique: the guiding information is provided regularly at the breathing cycle point that fits the cycle point during which the preoperative CT image was acquired (experiments in Part

IV confirm that this is actually the case).

Zhang et. al. and Maier-Hein et. al. [28,29] propose to insert additional needles in the liver to track its motion and then to predict the breathing movement whatever cycle point is chosen for the needle insertion. Accuracy results obtained on pigs showed the feasibility of their approach. However the clinical benefit of this interesting method is still questionable since introducing additional needles needs preprocedural time and represents further risk factor for the patient. That is why we have preferred to keep a respiratory gating technique to compensate for the liver motion.

We decided to provide the guiding information only during the expiratory phases of the patient. The preoperative CT image is acquired in accordance during an expiratory phase. Since the patient is intubated, the anesthetist can interrupt the breathing movement at expiratory phases during 20-30 sec. In this time interval, the practitioner can manipulate the needle toward the target. Obviously, during this short time interval, the registration of the model has to be performed as quickly as possible (typically, in less than a few seconds). This leads us to develop the following simple, robust and efficient techniques.

2.2 Automatic localization and matching of markers

These algorithms have already been published in [19], we summarize the main ideas here so that the paper remains self-content. Although markers are no longer the same as in [19], the principle remains similar. Moreover, the accuracy and robustness have been reevaluated and are very close to those in [19].

2.2.1 Automatic localization of 2D video markers

The principle of the marker localization in the video images is based on the intensity channel analysis and the assumption that skin takes up the main surface. Firstly, we find the skin in the video image, then an intensity thresholding around the skin intensity identifies potential markers. A size and shape analysis enables to select the markers among the connected components. Fig. 2 shows an example of marker extraction in a video image. Experiments performed on human torso showed that the extraction algorithm provides about 2% of false positive and 1% of false negative. The localisation accuracy was compared to a manual extraction performed by several users: an average error of 1.5 pixel has been reported. The extraction is performed at a 10 Hz rate on a 3.4GHz PC with 1GHz RAM (image size 800×600).

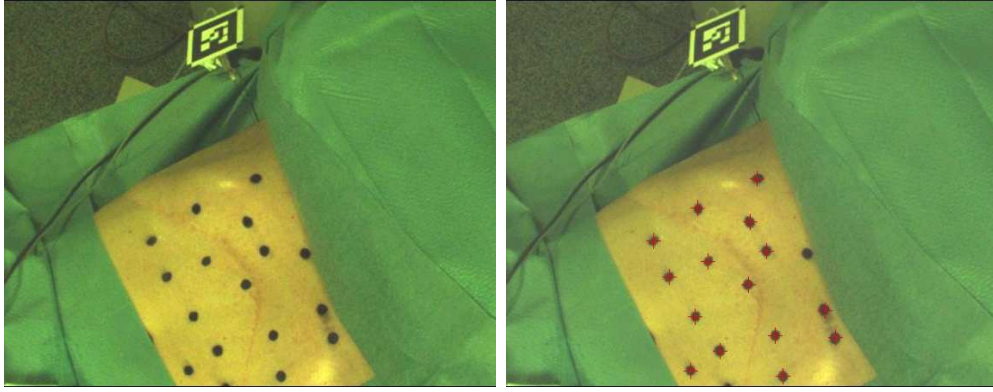


Fig. 2. Example of automatic detection of radio-opaque markers in a video image of a human abdomen. The extracted markers are indicated with red crosses

2.2.2 Automatic localization of 3D CT markers

Markers in the CT-image are extracted by a top-hat characterization [30] that emphasizes small singularities on the skin surface. An example of a marker extraction is given on Fig. 3. Experiments performed with in vivo data showed that the extraction algorithm provides about 3% of false positive and 5% of false negative. The extraction is performed in less than 30 sec. on a 3.4GHz PC with 1GHz RAM (image size of $512 \times 512 \times 150$ with a resolution of $1 \times 1 \times 2 \text{ mm}^3$).

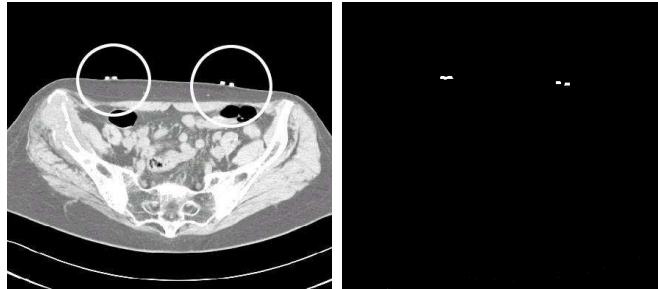


Fig. 3. Example of automatic detection of radio-opaque markers in a CT image of a human abdomen. Left: original image of the patient in grey level. Right: result of the image processing that emphasizes the marker position.

2.2.3 Automatic matching of 2D video markers

The matching between the video markers is realized thanks to epipolar geometry constraints. The matched markers are reconstructed in 3D in the camera reference frame. If erroneous 3D reconstructions due to false point matches appear, they are discarded by the subsequent video/CT matching procedure designed to be robust in the presence of such outliers.

2.2.4 Automatic matching of reconstructed video markers and CT markers

After reconstructing the set of 3D markers in the camera frame, we need to match them with the corresponding 3D points extracted from the CT-scan. We decided to use a prediction/verification algorithm [31] with additional distance constraints. This algorithm provides us not only with a matching estimation, but also a rough estimation of the transformation relating the CT and the camera frame.

When a correct transformation is found, we keep all the 3D/2D correspondences provided by the verification step to compute a more accurate transformation (see next paragraph). In this process, markers that were not matched in the previous step are implicitly reconsidered thanks to the verification. The matching experiments always provide a correct transformation, and 100% of the potential matches were found. The entire matching process took on average less than 1 second.

2.3 Registration of the virtual model in the camera frame

The markers being automatically extracted and matched, we now have to estimate accurately the rigid transformation T relating the CT frame with the camera frame. We choose a 3D/2D point registration approach to provide the rigid transformation that relates scanner frame and camera frame.

Since noise corrupts the 2D data and the 3D data, we optimize the *Extended Projective Points Criterion* (EPPC) (more details are given in [32]) on the transformation T and the *auxiliary variables* M_i :

$$EPPC(T, M_1, \dots, M_N) = \sum_{i=1}^N \frac{\|\tilde{M}_i - M_i\|^2}{2 \cdot \sigma_{3D}^2} + \sum_{k=1}^S \sum_{i=1}^N \xi_i^k \cdot \frac{\|\tilde{m}_i^{(k)} - m_i^{(k)}\|^2}{2 \cdot \sigma_{2D}^2}$$

where S (resp. N) is the number of cameras (resp. markers), $\tilde{m}_i^{(k)}$ is the observed 2D coordinates of the i^{th} markers in the k^{th} video image, \tilde{M}_i is the observed 3D coordinates of the i^{th} markers in the CT-image, M_i is the perfect 3D coordinates of the i^{th} markers in the CT-image, $m_i^{(k)} = P^{(k)}(T \star \tilde{M}_i)$, $P^{(k)}$ the projective function of the k^{th} camera, ξ_i^k is a binary variable equal to 1 if the i^{th} marker is visible in the k^{th} video image and 0 if not, and T the sought transformation. The minimization procedure is alternated w.r.t. the sought transformation T , and w.r.t. the M_i . Practically, registration on patient data is about 0.05 sec. with 15 markers and a rough initialization (provided by the latter matching algorithm).

An evaluation on patient data showed that the extraction and matching algo-

rithms are robust and that the overall computation time of the video extraction, matching and registration process is within 0.1 sec.

2.4 A simple and accurate needle tracking

Since the needle is no more visible when it is introduced under the skin, we have to track its position in the camera reference frame. To realize this, we rigidly attach a square marker on its top, and we localize in real-time its four corners using the ARTag library [33]. Then, knowing the size of the square, we are able to compute its position in the camera frame by minimizing the classical 3D/2D standard projective point criterion (SPPC)[32]. An accuracy evaluation (described in [34]), realized in simulated clinical conditions, showed that the average tracking error of the needle tip is within 1 mm.

3 In-vitro evaluation of the system accuracy and interface

In addition to the technical algorithms to track the needle and to register it to the patient model, we have to design an interface component to guide practitioners. Firstly, we describe the interface component designed with radiologists to be as ergonomic as possible. Secondly, we present a targeting experiment on an abdominal phantom that demonstrates the system efficiency in simulated clinical conditions.

3.1 A safe and ergonomic guidance interface

In the field of craniotomy, Grimson *et al* [35] superimpose the reconstructed model on external video images of the patient skull. In the interventional radiology context, this approach allows radiologists to check instantly that the rigid assumption is satisfied and that the patient did not slightly move. Indeed, a registration discrepancy of 2 mm can be clearly seen by practitioners in case of sliding or a skin deformation [36]. However, a guidance interface relying only on an external video view augmented with the patient model and the needle position does not seem to be optimal. In our previous system, such an interface was provided and practitioners complained that video views did not correspond to the their natural field of view and that real and visualized movements were often inverted. Therefore, an important interpretation effort was needed. Moreover, since the camera focals are fixed, no zoom of the area of interest is available.

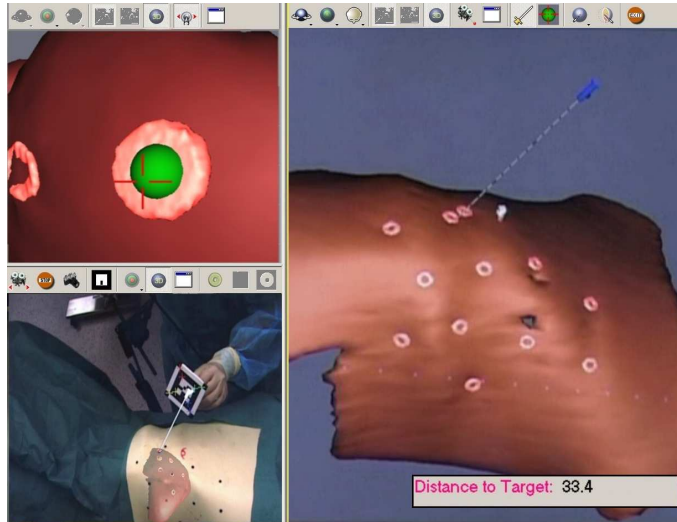


Fig. 4. Three screens of the guidance interface. The bottom left image corresponds to the augmented reality screen, in which the 3D reconstruction of the liver and the virtual needle are displayed. The top left image displays the virtual needle screen (oriented toward a marker stick on the liver surface). The right image shows the main virtual screen, in which one can see the relative position of the needle w.r.t. the phantom. We indicate in its corner the virtual distance in mm that separates the needle tip from the target (in this case, a marker center).

In the context of laparoscopy guidance, Marvik [37] proposed an interface that showed the tool position with respect to the 3D reconstructed model. In addition, they display the 3 CT-slices where the tip of the laparoscope lies. This approach is very useful for understanding of the relative position of the tool with respect to the model, since the user can choose his angle of view and an appropriated zoom. Nevertheless, it is not possible to assess in real time the quality of the registration during the intervention. Indeed, this can only be done interactively by pointing some reference points on the patient skin. That means that if the patient moves by 2 mm, the registration will undergo a 2 mm bias.

This analysis led us to develop an interface that provides both kinds of information. This interface (showed on Fig. 4) is divided into three screens, features and properties of which have been designed with practitioners, in order to provide them with a clear and intuitive tool. During needle insertion, the customization of each screen has to be done by a medical staff operator with a simple mouse action (organ color and transparency, virtual camera point of view...).

The augmented reality screen (bottom left image in Fig. 4)

In this screen, one of the two video images returned by our cameras is displayed. The practitioner can ask a medical assistant to switch between both camera views, to enable or disable the real-time superimposition of the 3D

model onto the video images, to choose the transparency level of its different elements and display the real-time extraction of markers. Furthermore, the medical assistant can superimpose the virtual needle on the tracked real needle and monitor the real-time tracking of the square marker attached on it. Finally, the practitioner can check visually the registration quality by observing the superimposition of the registered virtual markers.

The virtual needle screen (top left image in Fig. 4) In order to orient a tool toward a target, Carrat *et al* [38] proposed an interface that displays on a screen three crosses that have to be superimposed. The optimal trajectory is represented by a static central cross. Tool tip and axis are projected dynamically on a view orthogonal to this trajectory, and are represented by two different crosses.

To facilitate the orientation of the needle toward the target, we propose a similar tool: in the virtual needle screen, we display a view that corresponds to what a camera positioned on the needle tip and oriented along its axis would see. A cross indicates what the needle is oriented toward. In our interface, the 3D model of the tumor is visualized. If the practitioner defines in the CT a precise point he wants to reach, this target is represented by a 2 mm diameter green sphere. Radiologists told us that the 3D tumor model is an important information since following thoroughly the guidance information is not possible and the tumor shape visualization can influence their movement. To keep a good visibility when the needle goes through organs, modification of 3D model transparency can be performed.

The virtual exterior screen (right image in Fig. 4) In this screen, the 3D virtual scene, composed of the patient model and the tool representation, is rendered from a viewpoint controlled by the user. Like in a classical viewer, he can rotate, translate and zoom the elements and define their properties (visibility and transparency). Moreover, it is possible to also display the CT-scan from which the patient model is extracted, and navigate through its slices. The contrast can be enhanced like in a usual radiological viewer.

If the 3D models of liver and tumor are not available, for time or technical reasons, practitioners can visualize the 3D CT-slices instead. Then, they can define the target position on a specific CT slice by a mouse click (cf. Fig. 5). Since it is difficult to visually assess the distance between needle tip and target, we display the distance inside the virtual exterior view (see bottom right of the right screen on Fig. 4).

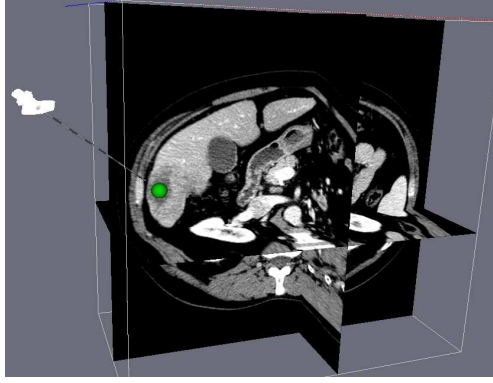


Fig. 5. Patient CT image displayed in the virtual exterior view. One can see a green sphere target that has been placed by the user.

3.2 Evaluation of the system on a static abdominal phantom

The purpose of the experiment is to assess the accuracy of the needle targeting and to show that the guiding interface is ergonomic. Four targets were modeled with radio-opaque markers stuck on the fake liver inside the phantom. Ten participants each performed 10 consecutive needle targetings of the model tumors (cf. Fig. 6 a). During the positioning, the operator placed the needle and stopped his movement when he thought that he had reached the tumor center. After each trial, the time required to position the needle was recorded, and a video snapshot of the needle position in the target was performed using an endoscopic camera introduced into the phantom and focusing on targets (cf. Fig. 6 b). Then, the accuracy of each needle targeting was assessed by three different operators and averaged. A quantitative measure was possible since the marker size is perfectly known in mm and can be converted into pixel. To assess the guidance interface, we asked practitioners to fill out a questionnaire on how they used the three screens and their usefulness during needle insertion. Accuracy and time results are shown in Table 1.

One can see that the worst average accuracy is below 3 mm, which clearly meets our accuracy constraint (5 mm). A previous experiment (described in [19]) in which the user was guided by an augmented reality screen only provided less accurate results, and more importantly longer manipulation times (59 sec. against 30 sec.). It confirms the fact that the complementarity of the three different screens is a powerful aspect of our interface. Unfortunately, our phantom does not allow to perform needle insertion experiments with the conventional CT scan procedure. Therefore we could not compare the insertion duration using our system and using the standard protocol.

The questionnaire raised the following points. Almost all radiologists used the *augmented reality view* at the beginning of the needle insertion to check the automatic skin fiducials detection, the visual quality of the skin registration,

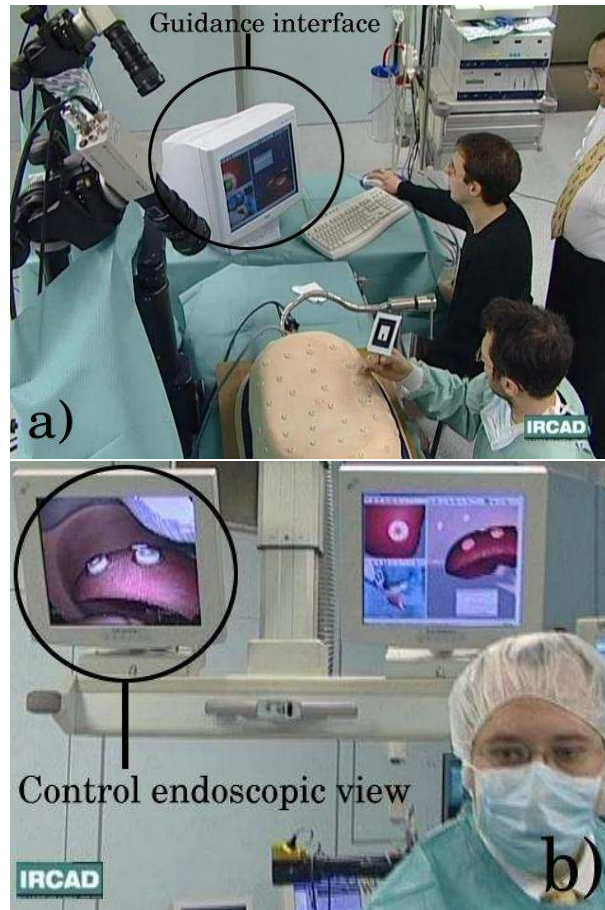


Fig. 6. a) Setup of the experiment: the user is positioning the needle, tracked by a stereoscopic system, thanks to the guidance interface. b) An endoscopic view is displayed behind the user. It allowed to visually measure the accuracy of each needle targeting.

and the tool superimposition. The ten radiologists used the *virtual needle view* to orientate correctly the needle before puncturing the phantom skin. During insertion, seven radiologists used the *virtual needle view* only. The three others preferred to use the *virtual exterior view* with a specific point of view they asked to the interface manipulator. When the radiologists were close to the target (typically below 5 mm), they all used the *virtual exterior view* with the help of another operator who zoomed on the interest zone and adapted the point of view to the requests of radiologists.

The distance in mm was almost never used nor considered as useful. This means that providing the distance information in such a way is not appropriate. A discussion with practitioners highlighted that a color coding of the tumor or a shrinking circle (like in [18]) may be a better solution to provide distance clues.

Practitioners also asked us whether it was possible to automatize the point

	Average distance (mm) \pm std.	Minimum distance	Maximum distance	Average time (sec.) \pm std.
Practitioner 1	1.5 \pm 0.45	1	3	24 \pm 10.2
Practitioner 2	2.6 \pm 1.10	0	5	36 \pm 5.0
Practitioner 3	2.3 \pm 1.23	0	3	25 \pm 4.1
Practitioner 4	2.5 \pm 0.77	0	3	35 \pm 5.6
Practitioner 5	1.9 \pm 0.95	0	4	39 \pm 4.0
Practitioner 6	2.2 \pm 0.84	0	3	18 \pm 5.5
Practitioner 7	1.4 \pm 1.10	0	3	25 \pm 5.9
Practitioner 8	1.7 \pm 0.81	0	2	19 \pm 2.7
Practitioner 9	1.7 \pm 0.92	0	3	32 \pm 6.5
Practitioner 10	2.0 \pm 1.03	1	4	26 \pm 4.5
All	1.98 \pm 0.5	-	-	28 \pm 7.0

Table 1

Accuracy and time results obtained by each user. The average distance, which is always below 3 mm, meets our accuracy constraints (5 mm). Moreover, the time needed is, by far, under 1 minute. However, this should not be compared to the 10 minutes needed for a standard intervention since the in-vitro conditions are quite different from the in-vivo ones.

of view selection in the *virtual exterior view*. Since there is an infinity of possibilities, they agreed that a fully automatic parameterization of the point of view will never satisfy them completely. However, they suggested that an automatic recentering with a remote interface (vocal or foot based) may be sufficient, so as to change the zoom and the point of view around the needle axis. This point is currently under study.

Finally, we propose an alternative interpretation of the accuracy results. The accuracy evaluated during this experiment corresponds to the cumulated error of needle tracking (of variance σ_{needle}^2), registration of the patient model (σ_{reg}^2) and practitioner skill to follow accurately the guiding information displayed by our system ($\sigma_{guidance}^2$). We showed in previous papers [32,34] that σ_{needle} is within 0.9 mm and that σ_{reg} is within 1.5 mm in these conditions. Consequently, we can estimate the order of magnitude of $\sigma_{guidance} \simeq \sqrt{1.98^2 - \sigma_{needle}^2 - \sigma_{reg}^2} \simeq 0.95$ mm. Although this result is probably underestimated since σ_{reg} and σ_{needle} may be correlated, it gives a qualitative idea of the guidance accuracy of the system.

4 Clinical experiments on patients

In the previous section we have showed that the system allows an accurate in vitro needle positioning and that the guidance interface was easy to use by practitioners. For the system to be used on patients, we still have to adapt it to the clinical environment and to evaluate its accuracy on patients. Since we kept in mind the clinical constraints when the system was developed for the in vitro evaluation, its adaptation was done easily and quickly. The evaluation step is obviously the most difficult and important one (cf. [39]).

In this section, we firstly enumerate the slight adjustments that were needed for our system to be introduced in the operating room. Secondly, we explain how the choice of specific patients allows us to develop a safe protocol to evaluate system robustness and accuracy. Finally, we present the experimental results obtained on 8 patients and demonstrate that the system error fits the clinical requirements when the guidance information is provided during expiratory phases.

4.1 A system adapted to the operating room constraints

4.1.1 A small and light pattern for needle tracking

The pattern attached to the needle has to be realized in sterilizable plastic. Its size has to be less than $6 \times 6 \times 3 \text{ cm}^3$, and its weight less than 50 grammes. Indeed, if the pattern is too large, it may touch the CT-ring when the needle is not deeply inserted (at the beginning of its positioning in the patient). If the pattern is too heavy, the needle may be bent after insertion and disturb the needle tracking that assumes the needle remains straight. Finally, we investigated different methods for attaching the sterile pattern to the needle. The first one required to thread the needle through a hole in the plastic. Although the plastic is sterilized, the radiologist considered that the needle tip must not touch anything before being inserted. In that case, a small particle could be scratched when the radiologist threads the needle without noticing it. The second method was accepted by the radiologist since it allows to attach directly the pattern on the plastic end part of the needle.

4.1.2 Visible and sterile markers during intervention

We stick plastic rings on the patient skin before the preoperative CT acquisition (these rings contain aluminium that generates no artefact). Then, we print a dot inside each ring marker with a black pen. After the CT acquisition, we remove the rings and use the black dots as markers. Since the patient ab-

domen is then sterilized with alcohol and betadine, the pen has to be indelible. To increase its indelibility, a nurse cleans up the patient skin with alcohol (it removes fat cells) before the pen marking.

We would have preferred using autostickable sterile markers. Unfortunately, such a product does not exist, and for our markers to be sterilized, we would have needed to use gas or ionization sterilization processes which are not used in our hospital (autoclava is the standard sterilization process).

4.2 A safe evaluation protocol with specific patients

Hepatic tumors sometimes need contrast agent to be injected in the patient to be visible in the CT modality. For these patients, the clinical protocol to target tumors in interventional CT is slightly different from the standard one. A preoperative CT acquisition of the abdomen is realized with contrast agent. To guide the needle, the practitioner performs a mental registration of interventional CT slices with the preoperative CT image (in which tumors are visible). When he thinks the needle is correctly positioned, a second CT acquisition with contrast agent of the patient abdomen is performed. This second CT acquisition allows the practitioner to check the needle position with respect to the tumor he targeted.

The additional images available for these patients allow us to perform a passive evaluation of our system using the following data acquisition protocol.

Experimental protocol:

- We stick radio-opaque markers on the patient skin and a black dot is printed inside them (cf. Fig. 2).
- A preoperative CT acquisition CT1 is realized in full expiration (it includes all the markers and the liver).
- Markers are removed from the skin.
- The practitioner attaches the sterile pattern to the needle.
- The practitioner inserts the needle without any advice or instruction from our system until he thinks he has correctly targeted the tumor.
- A stereoscopic video of the patient abdomen and needle is taken during several breathing cycles.

- A second CT acquisition CT2 is acquired in full expiration, the needle remaining in the patient (CT2 also includes the whole liver).

We highlight that this protocol does not change the information used by the practitioner to guide the needle: he realizes the intervention with his usual means (CT-slices) without any advice nor instruction from our system. In order to take our measures, we had to ask practitioners to attach a square marker on the needle, to stick radio-opaque markers on the patient, to set up our cameras in the operating room and to realize two apneas in expiratory phase. The potential impact on the intervention of these unusual conditions were considered negligible by the practitioner and the anesthetist.

From the acquired experimental data, we can not only evaluate the system accuracy but also check that the needle remains straight during the insertion and that the repositioning error of the abdominal structures at expiratory phases is negligible. To perform these three studies, we realize the three following evaluation processes:

Evaluation of the liver repositioning error:

- Extraction of spine, liver and skin in both CT1 and CT2.
- Registration of the spine from CT2 on the spine in CT1.
- Application of this registration to liver and skin from CT2. This registration allows to compare the relative movement of liver and skin with respect to a common rigid structure.
- Computation of the distance between the liver (resp. skin) surface in CT1 with the liver (resp. skin) surface extracted from CT2 and registered in CT1.

Fig. 7 summarizes this evaluation protocol.

Evaluation of the needle bending:

- Extraction of the needle in CT2
- Estimation of the needle direction for the first half and the second half of its length (see Fig.8)
- Comparison of both directions using the angular deviation α and the needle deflection.

Evaluation of the system accuracy:

- Extraction of liver and needle surfaces from CT2.
- Registration using ICP of the liver surface in CT2 on the liver surface in CT1.
- Application of the computed transformation to the needle surface extracted from CT2. This registration provides the final needle position in the CT1 image.
- Registration of the patient model from CT1 (with the needle) in the camera reference frame using the video image of the patient at full expiration.
- Discrepancy evaluation between the needle tracked by the camera (at expi-

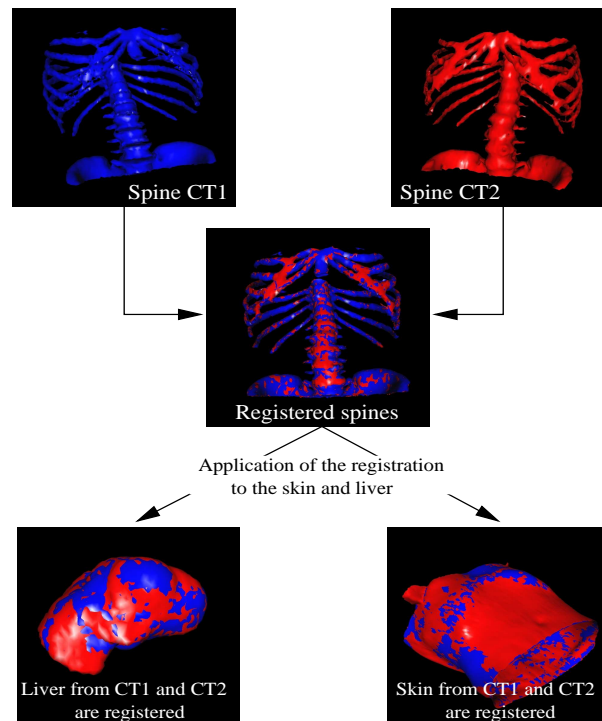


Fig. 7. To evaluate the repositioning error of liver and skin we firstly register the spines from CT1 and CT2. Then we apply the found rigid transformation to liver and skin surfaces and measure the distance between both surfaces.

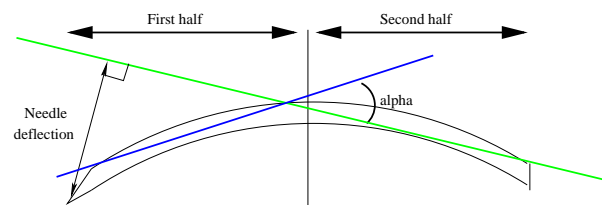


Fig. 8. To estimate the needle bending, we split its CT segmentation in two halves.

ration phase) and the needle registered in CT1.

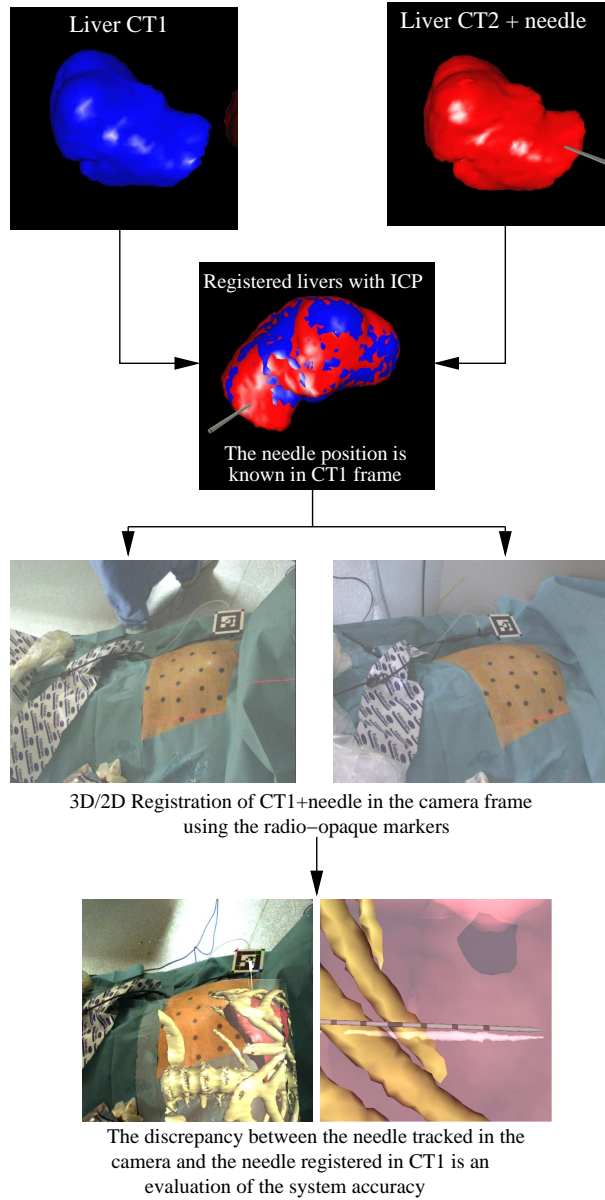


Fig. 9. Illustration of the passive protocol to evaluate the system accuracy.

Fig. 9 summarizes this evaluation protocol. We emphasize that this discrepancy is an evaluation of the cumulated error of σ_{needle}^2 , σ_{reg}^2 , and the repositioning error σ_{rep}^2 . It does not include the error $\sigma_{guidance}^2$ that corresponds to the ability of practitioners to follow the guiding information provided by the system. Consequently, our experimental protocol allows to evaluate all error sources that only depend on the system and not on practitioner ability². Al-

² In fact, we measure a slight over-estimation of σ_{system} since the needle registration from CT2 to CT1 is not perfect although of high quality (we will check it in the next section).

ternatively, the measured error corresponds to the final system error if the needle insertion is robotized (in that case $\sigma_{guidance}^2$ is negligible).

4.3 Evaluation of the system on eight clinical cases

Eight patients (6 males and 2 females, aged between 50 and 60) have participated in our experiments after signing an informed consent. They all had tumors, the diagnosis of which led to a thermal ablation. Resolution of CT images was $1 \times 1 \times 2mm^3$. Below are presented the results obtained for the three experimental evaluations described in the previous subsection.

4.3.1 Verification of the needle rigidity assumption

The needle is firstly segmented in the CT2 acquisition using an interactive localization followed by an intensity threshold. Then, we evaluate the orientation of its first half and its second half (cf. Fig. 8) and compute the angular difference α between both orientations and the needle deflection. The practitioner sometimes bends the needle on purpose to avoid a critical structure. For all the reported cases, the practitioner estimated that this was not the case. Consequently, we are measuring here the uncontrollable bending of the needle.

One can see in Tab. 2 that the needle deflection is not negligible in 25% of cases as it can reach 2.5 mm. Since the system assumes that the needle remains straight, the needle tip position provided by the system is systematically biased when there is an important deflection. Visual illustrations of needle deflections are provided on Fig. 10.

Patient Nb	1	2	3	4	5	6	7	8
Angular deviation alpha ($^\circ$)	1.0	2.8	0.5	0.6	1.1	1.8	0.9	1.0
Needle deflection (mm)	0.85	2.5	0.4	0.5	1.0	1.82	0.6	0.7

Table 2

Evaluation of the needle bending after its positioning in the patient.

4.3.2 Evaluation of the organ repositioning error σ_{rep}

To quantify the distance between two registered surfaces S_1 and S_2 , we compute the RMS of the distance between each point on S_i to the surface S_j :

$$d(S_1, S_2) = \sqrt{\frac{\sum_{M_i \in S_1} d(M_i, S_2)^2 + \sum_{P_i \in S_2} d(P_i, S_1)^2}{2 \cdot (\text{card}(S_1) + \text{card}(S_2))}}$$

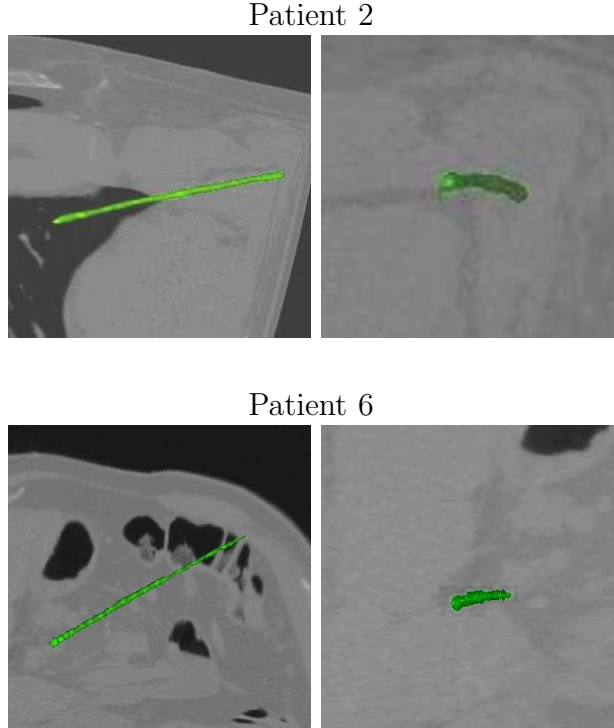


Fig. 10. Illustration of the needle bending for patients 2 and 6. Left: lateral view of the needle. Right: axial view of the same needle to highlight its important bending.

where the distance $d(M_i, S)$ between a point M_i and a surface S is interpolated from the 3 closest points of M_i belonging to S . Tab. 3 provides the distance between the registered surface from CT2 in the frame of CT1.

Patient Nb	1	2	3	4	5	6	7	8	Average
Spine $d(S_1, S_2)$ in mm	0.8	0.8	0.9	0.9	1.1	1.2	0.7	1.1	0.94
Liver $d(S_1, S_2)$ in mm	1.5	1.2	1.4	1.7	1.5	1.8	1.2	1.6	1.48
Skin $d(S_1, S_2)$ in mm	1.6	1.8	2.9	1.8	3.2	1.7	1.5	1.9	2.05

Table 3

Distance between the registered surfaces of spine, liver and skin.

One can see that the distance between the liver surfaces is within 2 mm for each patient which is of the same magnitude as the segmentation uncertainty [40,34]. To check that the measured distances are not due to a pure translation, we display the relative position of both surfaces. Fig. 11 shows clearly that surfaces are closely interlaced for all patients. This suggests that the observed distance is essentially due to the segmentation error in the CT acquisitions.

Oddly, distances between skin surfaces are not very low for each patient. A visual check (see Fig. 12) of registered surfaces shows that for these patients the skin of the lower part of the abdomen has moved between both CT acquisitions. An inspection of both CTs indicates that a movement of gas or/and

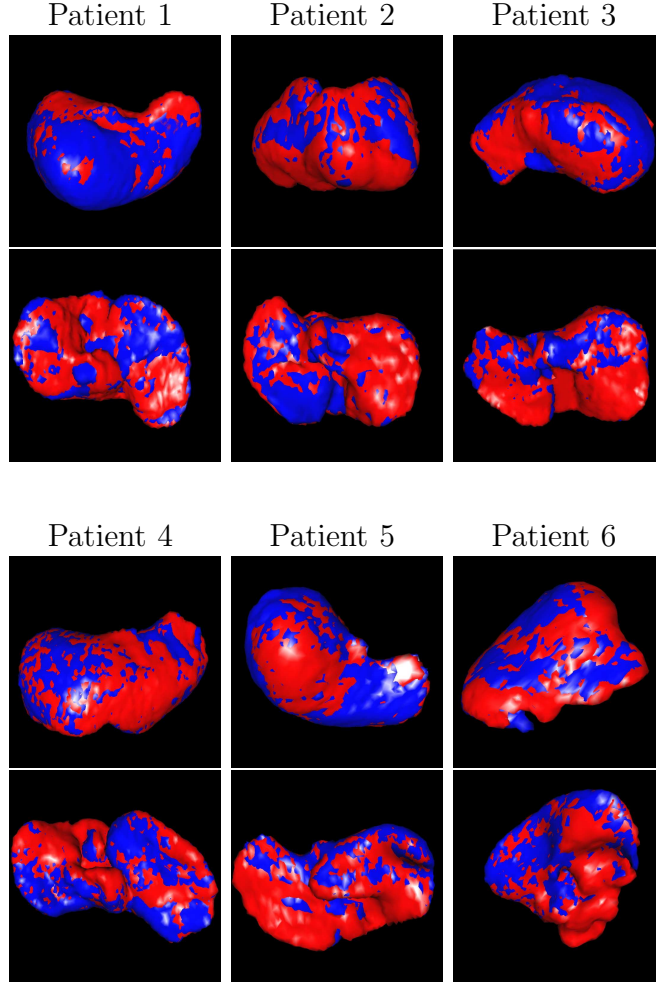


Fig. 11. Visual check of the liver repositioning error on 6 patients. Two opposite views of registered surfaces are provided for each patient. One can see that registered surfaces are closely interlaced. This means that the repositioning error of the liver is close to the segmentation error, i.e. 1 mm.

bowels was responsible for this deformation (see Fig. 13). We highlight that this skin deformation highly disturbs the system if we take the radio-opaque markers on the deformed zone into account to compute the patient model registration. Indeed, the system implicitly assumes that the relative position of the liver w.r.t. the markers remains rigid during the intervention. Consequently, the skin deformation can lead to a wrong estimation of the liver position.

We notice that this phenomenon essentially happened when practitioners used the US probe. In practice, if our system is used for needle positioning, a US probe should not be necessary. However, if a US probe has to be manipulated, the system should be carefully used. In such a case, radio-opaque markers should be stuck on the upper part of the abdomen only, which is a zone that is not influenced by gas movements.

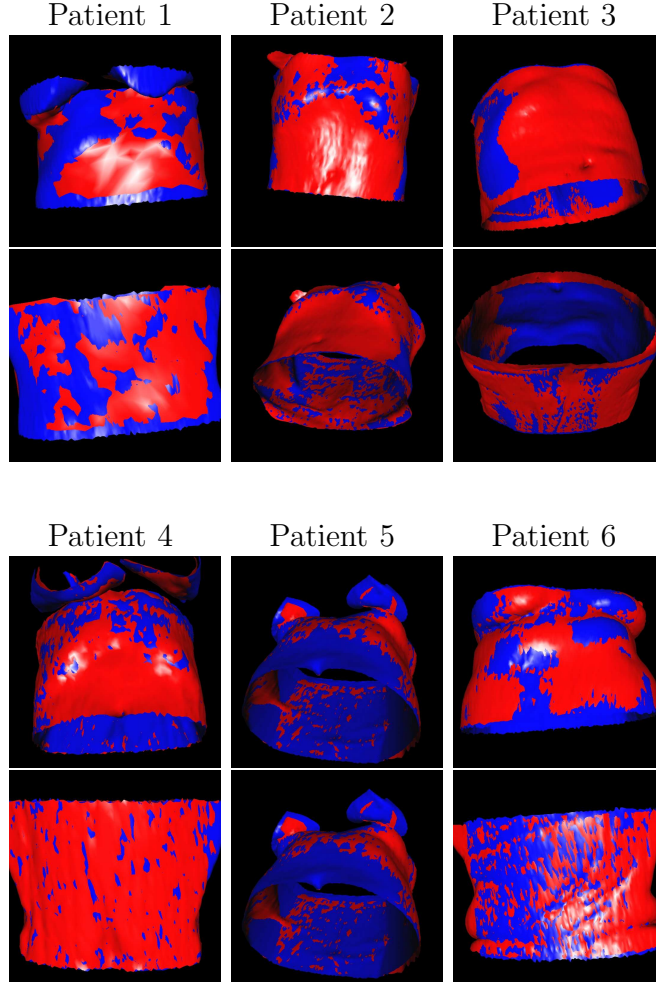


Fig. 12. Visual check of the skin repositioning error on 6 patients. Two opposite views of registered surfaces are provided for each patient. One can see that registered surfaces are closely interlaced on the patient back. For some patients (2,3,4 and 5), the abdominal skin surfaces are not interlaced at all. A slight translation antero-posterior within 1 mm explained this phenomenon for patients 2 and 4, whereas for patients 3 and 5 it was due to gas and bowel movements.

4.3.3 Influence of breathing on the system accuracy

During the 8 interventions, the needle and the patient were video tracked along several breathing cycles. Because of the gas and bowel movements that we observed on two patients, we choose not only to report the system accuracy using all markers but also using the subset of markers that are not on the lower abdominal part. From the CT images we empirically observed that only the markers below the lower part of the liver had an influence on the registration algorithm.

Tab. 4 shows for each patient the system accuracy, the 3D/2D and 3D/3D registration error of CT markers on the video markers averaged on expiratory

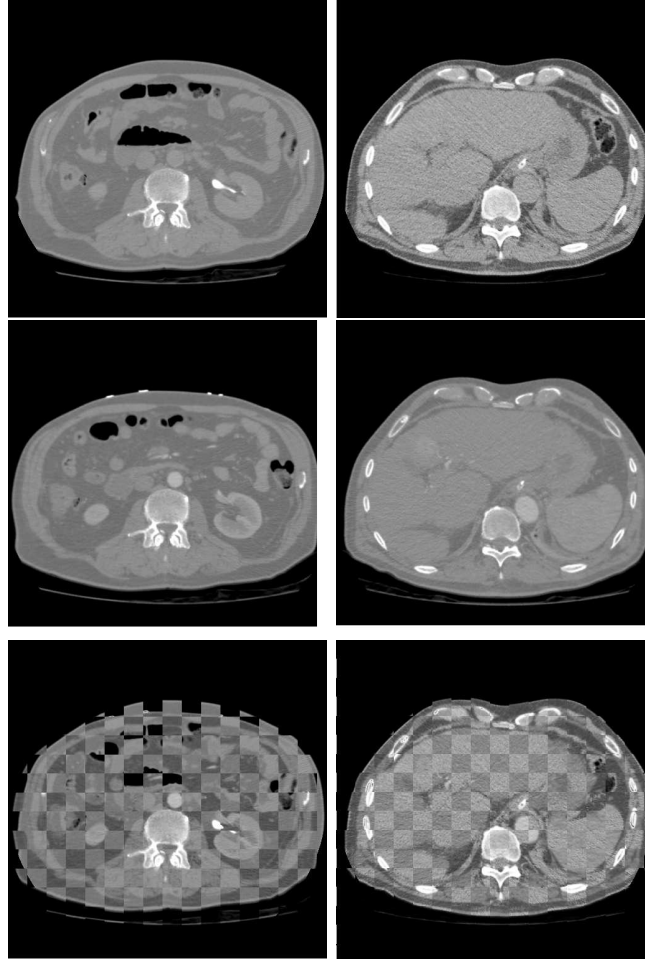


Fig. 13. Illustration of the skin deformation due to gas movement in the bowels. Top left (resp. right) images: slice from CT1 in the lower (resp. upper) part of the abdomen. Middle left (resp. right) images: slice from CT2 in the lower (resp. upper) part of the abdomen. Bottom images: superimposition of the slices from CT1 and CT2. One can see that the skin deformation is important in the lower part of the abdomen (skin and bowels have moved) whereas it is very low around the upper ribs (skin and liver edge are almost identical).

phases that were video recorded. Additionally, we report in Fig. 14 a sample for patients 1 and 2 during 4 breathing cycles of the system accuracy, the 3D/2D and 3D/3D registration error.

Results in Tab. 4 clearly indicate that the system accuracy during expiratory phases reaches 4.2 mm on average for patients who did not undergo gas and/or bowel movements (patients 3 and 5). We highlight that if only the markers above the liver are used for registration, the system accuracy remains acceptable (average of 5.1 mm). This means that if viscera movement are suspected, removing the markers below the liver from the registration inputs will still provide a sufficient accuracy. Note that an important shape deformation can be detected using the 3D/3D registration RMS that increases above 2 mm

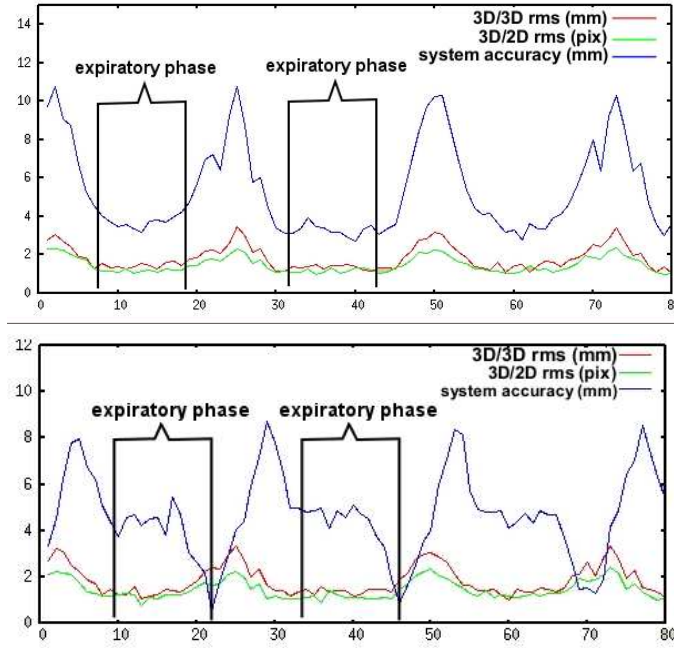


Fig. 14. Sample of system accuracy and registration errors reported during several breathing cycles with patients 1 and 2.

	Number of markers used	RMS 3D/2D (pixel)	RMS 3D/3D (mm)	System accuracy (mm)
Patient 1	15 (8)	1.3 (1.1)	1.5 (1.3)	4.0 (4.9)
Patient 2	13 (7)	1.0 (0.9)	1.7 (1.4)	4.2 (4.8) [3.5]
Patient 3	15 (6)	2.2 (1.2)	2.5 (1.4)	14.5 (5.2)
Patient 4	12 (7)	1.5 (1.3)	1.2 (1.0)	4.1 (5.0)
Patient 5	13 (8)	2.0 (0.9)	2.4 (1.5)	12.3 (4.8)
Patient 6	14 (9)	1.2 (1.1)	1.2 (1.1)	4.3 (5.1) [3.9]
Patient 7	15 (8)	1.3 (1.1)	1.8 (1.5)	4.4 (5.1)
Patient 8	14 (9)	1.1 (1.0)	1.7 (1.4)	4.1 (5.0)
Average	13.8 (7.7)	1.45 (1.1)	1.75 (1.32)	4.2 (5.1)

Table 4

Average for each patient of the system error, 3D/2D and 3D/3D registration errors during expiration phases. Values in brackets correspond to the results obtained when only the markers above the liver are used for the registration. Values in square brackets correspond to the system accuracy re-evaluated after a compensation of the important needle bending (only for patients 2 and 6). The average system accuracy with all markers does not include the results of patient 3 and 5.

during the entire breathing cycle.

For patients in whom the needle was bent, we have evaluated the system accuracy while taking the observed bending into account. Then, we observed that if the rigidity assumption of the needle was true, the system accuracy would be slightly better (about 0.6 mm).

One can see in Fig.14 that RMS errors evolve cyclically, as expected, and are always minimal in expiration phases. The system accuracy also evolves cyclically but is not always minimal in expiration phases. Indeed, since the patient model registration is not perfect, the system can register the needle extracted from the CT at a position that corresponds to an intermediate phase of the breathing cycle (whereas it should be registered at expiratory position).

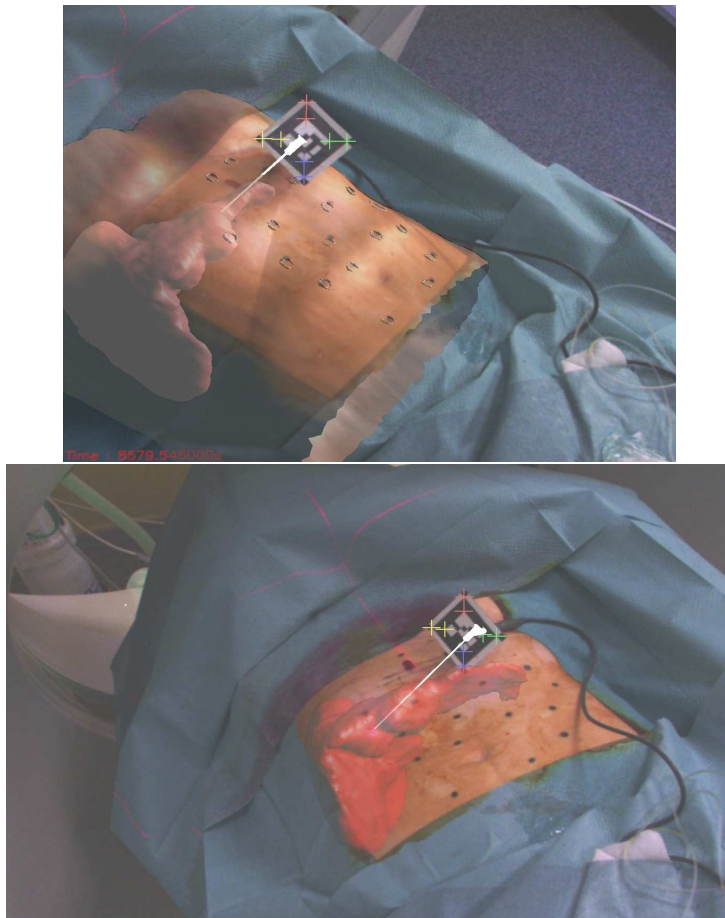


Fig. 15. Augmented reality view of the patient 1. The registration was done with 15 markers. Left image: skin and liver models are superimposed on the video image. Right image: only the liver is superimposed in transparency. One can see that the black dots are still highly visible despite the skin sterilization.

Finally, we provide in Tab. 5 the amplitude of the needle motion due to breathing after its insertion. We sample on Fig. 16 the trajectory of a needle tip (patient 1, 7 cm in depth) during several breathing cycles. The major movement

is always along the cranio-caudal axis with a magnitude around 13 mm and a repositioning error of 1.2 mm. These results are consistent with the existing studies on the liver movement during shallow breathing [21–24].

Fig. 15 shows the augmented reality views obtained during the intervention on patient 1. One can distinguish the needle position inside the liver.

	anterior posterior (mm)	lateral (mm)	cranio caudal (mm)	total (mm)	repositioning error (mm)
Patient 1	2	2.2	10.5	10.9	1.2
Patient 2	1.9	2.1	13.4	13.7	1.4
Patient 3	1.2	1.9	15.2	15.3	1.0
Patient 4	1.4	2.3	9.5	9.8	1.1
Patient 5	1.8	2.1	11.9	12.2	1.7
Patient 6	2.1	2.2	12.3	12.7	1.2
Patient 7	2.3	1.9	14.3	14.6	1.5
Patient 8	2.0	2.3	16.8	17.1	1.7
Average	2.1	2.2	12.8	13.5	1.34

Table 5
Evaluation of the motion amplitude of the needle tip once inserted.

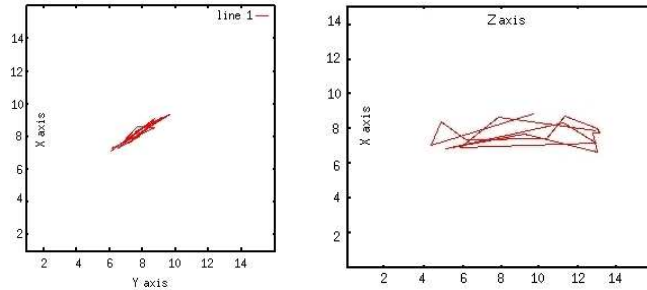


Fig. 16. Trajectory of the needle tip during 4 breathing cycles of the patient 1 as measured by our tracking system. The needle was inserted 7 cm in depth and the patient was under general anesthesia. The main movement is along the cranio-caudal axis Z (1 cm).

5 Conclusion

We have developed a video based augmented reality system to guide liver percutaneous punctures in interventional radiology. This system tracks in real-

time the puncture needle and automatically registers (at a 10 Hz rate) the 3D preoperative patient model in the camera frame using radio-opaque markers stuck on the skin. The patient model is reconstructed from a 3D CT-scan realized just before the intervention. To take the breathing motion issue into account, we use a respiratory gating technique. We synchronize the preoperative CT acquisition and the guidance step with the expiratory phases of the patient. Then, we assume *pseudo static* conditions and rigidly register the patient model.

A preliminary experiment realized on an abdominal phantom showed that a 2 mm targeting accuracy could be achieved within 30 seconds in vitro, showing that the interface design (realized with practitioners) allows a quick needle positioning and that the registration process is accurate enough under the rigidity assumption.

It is crucial for practitioners to know the system accuracy on patients in clinical conditions since it modifies their state of mind during an intervention. Indeed, if the system error is below 2 mm, practitioners can totally rely on the information provided, whereas if it is beyond 10 mm, they may use the system only to reinforce their initial opinion. However, an accuracy evaluation is difficult to perform in the absence of ground truth data. In the last part we propose a passive protocol on carefully chosen patients that allows to obtain a ground truth CT at the end of the needle insertion. It allows us to rigorously assess the system accuracy on real patients and the *pseudo static* assumption along the intervention. Experimental results firstly show that the liver repositioning error is about 1 mm although it is sometimes much more important for the skin because of gas and/or bowel movements. This phenomenon can dramatically decrease the system accuracy if markers on the deformed zone are used to compute the patient model registration. This phenomenon can be detected by monitoring the 3D/3D registration RMS that increases in case of skin deformation. In that case, we show that removing the markers below the liver from the registration allows to maintain sufficient accuracy. Secondly, we have evaluated that the needle bending can cause a needle tracking error above 2 mm (although the practitioner thought it was not bent). Despite these uncertainties, we have finally evaluated our system accuracy during the patient expiratory phases at about 4.5 mm, what fits medical requirements. To our knowledge, it is the first time that a guiding system in interventional radiology for liver puncture is evaluated on real patients under clinical conditions corresponding to the focused application.

To avoid sticking radio-opaque markers, we are now investigating a structured light approach to recover in real-time the surface of the patient skin during the intervention. To reduce the inaccuracies due to the needle bending, we would like to add a fast segmentation tool that would allow to measure the needle bending from several preoperative CT slices and to compensate for it when

using the system. Secondly, we plan to investigate the integration of an electromagnetic tracker in the current system and to evaluate its accuracy when ferromagnetic distortions are compensated (using for example the method in [41]). However, in order to be useful in our system, such an EM tracker should have an accuracy better than 2 mm. Finally, we are confident that this system associated with a breathing motion simulator such as the one recently described in [42] could provide an accurate guidance information during the entire breathing cycle of the patient.

References

- [1] J. McGahan, G. Dodd III, Radiofrequency ablation of the liver: Current status, *American Journal of Roentgenology* 176 (1) (2001) 3–16.
- [2] S. Curley, Radiofrequency ablation of malignant liver tumors, *Annals of Surgical Oncology* 1 (2003) 338–347.
- [3] P. L. Pereira, Actual role of radiofrequency ablation of liver metastases, *European Radiology* 7 (2007) 291–299.
- [4] M. Loser, N. Navab, A new robotic system for visually controlled percutaneous interventions under CT fluoroscopy, in: *Medical Image Computing and Computer Assisted Intervention (MICCAI'00)*, Vol. 1935 of *Lecture Notes in Computer Science*, Springer, 2000, pp. 887–896.
- [5] G. Corral, L. Ibáñez, C. Nguyen, D. Stoianovici, N. Navab, K. Cleary, Robot control by fluoroscopic guidance for minimally invasive spine procedures, in: *Computer Assisted Radiology and Surgery (CARS 2004)*., Vol. 1268 of *International Congress Series*, Elsevier, 2004, pp. 509–514.
- [6] A. Patriciu, M. Awad, S. Solomon, M. Choti, D. Mazilu, L. Kavoussi, D. Stoianovici, Robotic assisted radio-frequency ablation of liver tumors: a randomized patient study, in: *Springer-Verlag (Ed.), Heigth International Conference on Medical Image Computing And Computer-Assisted Intervention (MICCAI'05)*, Vol. LNCS 3750, 2005, pp. 526–533.
- [7] G. Fichtinger, T. DeWeese, A. Patriciu, A. Tanacs, D. Mazilu, J. Anderson, K. Masamune, R. Taylor, D. Stoianovici, System for robotically assisted prostate biopsy and therapy with intraoperative CT guidance, *Journal of Academic Radiology* 9 (1) (2002) 60–74.
- [8] E. Boctor, R. Taylor, G. Fichtinger, M. Choti, Robotically assisted intraoperative ultrasound with application to ablative therapy of liver cancer, in: *SPIE Annual Conference on Medical Imaging 2003*, Vol. 5029, 2003, pp. 281–291.
- [9] B. Maurin, C. Doignon, J. Gangloff, B. Bayle, M. de Mathelin, O. Piccin, A. Gangi, CT-Bot: A stereotactic-guided robotic assistant for percutaneous

procedures of the abdomen, in: in Proc. SPIE Medical Imaging 2005, San Diego, USA, 2005, pp. 241–250.

- [10] M. Clifford, F. Banovac, E. Levy, K. Cleary, Assessment of hepatic motion secondary to respiration for computer assisted interventions, *Computer Aided Surgery* 7 (5) (2002) 291–299.
- [11] M. Rosenthal, A. State, J. Lee, G. Hirota, J. Ackerman, K. Keller, E. Pisano, M. Jiroutek, M. Keith, H. Fuchs, Augmented reality guidance for needle biopsies; an initial randomized, controlled trial in phantoms, *Medical Image Analysis* 6 (3) (2002) 313–320.
- [12] F. Sauer, A. Khamen, B. Bascle, L. Schimmang, F. Wenzel, S. Vogt, Augmented reality visualization of ultrasound images: System description, calibration, and features, in: Proc. of IEEE and ACM International Symposium on Augmented Reality (ISAR'01), New-York, 2001, pp. 30–39.
- [13] G. Stetten, D. Shelton, W. Chang, V. Chib, R. Tamburo, D. Hildebrand, L. Lobes, J. Sumkin, Towards a clinically useful sonic flashlight, in: Proc. of IEEE International Symposium on Biomedical Imaging, 2002, pp. 417–420.
- [14] M. Mitschke, A. Bani-Hashemi, N. Navab, Interventions under video-augmented X-ray guidance: Application to needle placement, in: Third International Conference on Medical Image Computing And Computer-Assisted Intervention (MICCAI'00), Vol. LNCS 1935, Pittsburgh, Pennsylvania USA, 2000, pp. 858–868.
- [15] B. Bascle, N. Navab, M. Loser, B. Geiger, R. Taylor, Needle placement under X-ray fluoroscopy using perspective invariants, in: I. C. S. Press (Ed.), Proceedings of IEEE Workshop on Mathematical Methods in Biomedical Image Analysis (MMBIA'00), 2000, pp. 46–53.
- [16] G. Fichtinger, K. Massamune, A. Deguet, H. Mathieu, R. H. Taylor, E. Balogh, J. Zinreich, L. Fayad, G. Fischer, Image overlay guidance for needle insertion in ct scanner, *IEEE Transaction on Biomedical Engineering* 52 (8) (2005) 1415–1424.
- [17] G. Fichtinger, A. Deguet, K. Masamune, E. Balogh, G. Fischer, H. Mathieu, R. Taylor, L. Fayad, Z. S.J., Needle insertion in CT scanner with image overlay - cadaver studies, in: Seventh International Conference on Medical Image Computing And Computer-Assisted Intervention (MICCAI'04), LNCS 3217, Springer-Verlag, 2004, pp. 795–803.
- [18] S. Vogt, F. Wacker, A. Khamene, D. Elgort, T. Sielhrst, H. Niemann, J. Duerk, J. Lewin, F. Sauer, Augmented reality system for MR-guided interventions: phantom studies and first animal test, in: R. L. Galloway (Ed.), Proceedings of SPIE Medical Imaging: Visualization, Image-Guided Procedures, and Display, Vol. 5367, 2004, pp. 100–109.
- [19] S. Nicolau, A. Garcia, X. Pennec, L. Soler, N. Ayache, An augmented reality system to guide radio-frequency tumor ablation, In *Journal of Computer Animation and Virtual World* 16 (1) (2005) 1–10.

- [20] J. Balter, K. Lam, C. McGinn, T. Lawrence, R. Ten Haken, Improvement of CT-based treatment-planning models of abdominals targets using static exhale imaging, *Int. J. Radiation Oncology Biol. Phys.* 41 (4) (1998) 939–943.
- [21] J. Wong, M. Sharpe, D. Jaffray, V. Kini, J. Robertson, J. Stromberg, A. Martinez, The use of active breathing control (ABC) to reduce margin for breathing motion, *Int. J. Radiation Oncology Biol. Phys.* 44 (4) (1999) 911–919.
- [22] L. Dawson, K. Brock, S. Kazanjian, D. Fitch, C. McGinn, T. Lawrence, R. Ten Haken, J. Balter, The reproducibility of organ position using active breathing control (ABC) during liver radiotherap, *Int. J. Radiation Oncology Biol. Phys.* 51 (2001) 1410–1421.
- [23] V. Remouchamps, F. Vicini, M. Sharpe, L. Kestin, A. Martinez, J. Wong, Significant reductions in heart and lung doses using deep inspiration breath hold with active breathing control and intensity-modulated radiation therapy for patients treated with locoregional breast irradiation, *Int. J. Radiation Oncology Biol. Phys.* 55 (2003) 392–406.
- [24] R. Wagman, E. Yorke, E. Ford, P. Giraud, G. Mageras, B. Minsky, K. Rosenzweig, Respiratory gating for liver tumors: use in dose escalation, *Int. J. Radiation Oncology Biol. Phys.* 55 (3) (2003) 659–668.
- [25] E. Lermite, J. Lebigot, F. Oberti, P. Pessaux, C. Aube, P. Cales, J. Arnaud, Radiofrequency thermal ablation of liver carcinoma, *Gastroenterology Clinical Biology* 30 (2006) 130–135.
- [26] M. Sawada, S. Watanabe, H. Tsuda, T. Kano, An increase in body temperature during radiofrequency ablation of liver tumors, *Anesthesia and Analgesia* 94 (2002) 1416–1420.
- [27] L. Soler, H. Delingette, G. Malandain, N. Ayache, J. Marescaux, Fully automatic anatomical, pathological, and functional segmentation from CT scans for hepatic surgery, *Computer Aided Surgery* 6 (3) (2001) 131–142.
- [28] H. Zhang, F. Banovac, N. Glossop, K. Cleary, Two-stage registration for real-time deformable compensation using an electromagnetic tracking device, in: *Medical Image Computing and Computer-Assisted Intervention. MICCAI 2005*, Vol. LNCS 3750, 2005, pp. 992–999.
- [29] F. Maier-Hein, L. Pianka, A. Seitel, S. Mller, A. Tekbas, M. Seitel, I. Wolf, B. Schmied, H. Meinzer, Precision targeting of liver lesions with a needle-based soft tissue navigation system, in: *Medical Image Computing and Computer-Assisted Intervention. MICCAI 2007*, Vol. LNCS 4792, 2007, pp. 42–49.
- [30] P. Soille, *Morphological Image Analysis*, 2nd Edition, Springer, 2002.
- [31] N. Ayache, O. Faugeras, HYPER: A new approach for the recognition and positioning of 2D objects, *IEEE Transactions on Pattern Analysis and Machine Intelligence* 8 (1) (1986) 44–54.

- [32] S. Nicolau, X. Pennec, L. Soler, N. Ayache, An accuracy certified augmented reality system for therapy guidance, in: European Conference on Computer Vision (ECCV'04), LNCS 3023, Springer-Verlag, 2004, pp. 79–91.
- [33] M. Fiala, ARTag, an improved marker system based on ARToolkit, NRC/ERB-1111 NRC 47166, National Research Council Canada (July 2004).
URL <http://www.artag.net/>
- [34] S. Nicolau, Un système de réalité augmentée pour guider les opérations du foie en radiologie interventionnelle, Ph.D. thesis, Université de Nice - Sophia Antipolis (Nov. 2004).
- [35] W. Grimson, G. Ettinger, S. White, W. W. T. Lozano-Perez, R. Kikinis, An automatic registration method for frameless stereotaxy, image-guided surgery and enhanced reality visualization, *IEEE Trans. Medical Imaging* 15 (2) (1996) 129–140.
- [36] J. Fitzpatrick, D. Hill, Y. Shyr, J. West, C. Studholme, C. Maurer, Visual assessment of the accuracy of retrospective registration of MR and CT images of the brain, *IEEE Transactions on Medical Imaging* 17 (4) (1998) 571–585.
- [37] R. Marvik, T. Lang, G. Tangen, J. Andersen, J. Kaspersen, B. Ystgaard, E. Sjlíe, R. Fougner, H. Fjsne, T. Hernes, Laparoscopic navigation pointer for 3-D image guided surgery, *Surgical Endoscopy* 18 (8) (2004) 1242–1248.
- [38] L. Carrat, J. Tonetti, P. Merloz, J. Troccaz, Percutaneous computer-assisted iliosacral screwing: Clinical validation, in: S. Verlag (Ed.), Third International Conference on Medical Image Computing And Computer-Assisted Intervention (MICCAI'00), Vol. LNCS 1935, 2000, pp. 1229–1237.
- [39] P. Jannin, J. Fitzpatrick, D. Hawkes, X. Pennec, R. Shahidi, M. Vannier, Validation of medical image processing in image-guided therapy, *IEEE Transactions on Medical Imaging* 21 (12) (2002) 1445–1449.
- [40] R. Anxionnat, M.-O. Berger, E. Kerrien, S. Bracard, L. Picard, Intra- and inter-observer variability in the angiographic delineation of brain arterio-venous malformations (avms), in: 17th International Congress and Exhibition on Computer Assisted Radiology and Surgery - CARS'2003, Londres, Royaume-Uni, Elsevier, 2003, pp. 1297–1298.
URL <http://www.loria.fr/publications/2003/A03-R-180/A03-R-180.ps>
- [41] A. Chung, P. Edwards, F. Deligianni, G. Yang, Freehand cocalibration of optical and electromagnetic trackers for navigated bronchoscopy, in: *Medical Imaging and Augmented Reality: Second International Workshop, MIAR2004.*, Vol. LNCS 3150, 2004, pp. 320–328.
- [42] A. Hostettler, S. Nicolau, L. Soler, Y. Remond, A real-time predictive simulation of abdominal organs position induced by free breathing, in: *Proceedings of ISBMS*, Vol. LNCS 5104, Springer, 2008, pp. 89–97.